

Validation of High-Throughput Wound Healing Assay Using 3D Cell Patterning and Automated, Kinetic Imaging



Authors

Brad Larson and
Peter Banks, PhD
Agilent Technologies, Inc.
Winooski, VT, USA

Glauco R. Souza and
William Haisler
Nano3D Biosciences, Inc.
Houston, TX, USA

Jan Seldin
Greiner Bio-One
Monroe, NC, USA

Introduction

Wound healing, both acute and chronic, involves a complex internal and external choreography of signaling, in addition to interactions with neighboring cells and the surrounding environment or external stimuli, and cell migration. This synergistic relationship can also vary depending on the wound type. Therefore, characterizing the mechanisms therein is of great interest for many applications, including wound dressing, burn and ulcer healing, scar elimination, anti-aging and aesthetic cosmetics, and much more. Historically, most wound healing assays use a scratch technique, where a confluent two-dimensional (2D) cell layer is mechanically injured, and cell migration is measured. Major limitations of this method are the lack of biomimetic environment, *in vivo*-like architecture and multicellular network, and as scratching methods vary, results are difficult to replicate. Newer three-dimensional (3D) methods allow cells to self-aggregate in the absence of a solid substrate. Vital cell-cell and cell-extracellular matrix (ECM) communication networks are able to be re-established. In this way, both cellular morphology and behavior more closely mimic that found in the body.

This application note demonstrates a novel 3D wound healing assay model (Figure 1) that can overcome 2D assay limitations. The method incorporates magnetic levitation where cells are first incubated with a nontoxic, magnetic nanoparticle assembly consisting of gold, iron oxide, and poly-L-lysine, which magnetizes the cells without inducing an inflammatory cytokine response. The cells are then placed into a microplate well and levitated by placing a magnet above the well. The cells aggregate and form ECM within a few hours, the magnet is removed, and pipetting is performed to break up the aggregate, once again creating a single cell suspension. Appropriate cell numbers are then transferred to a 384-well assay plate and a ring magnet drive is positioned below the plate, allowing the cells within each well to be patterned into a new 3D ring shape. Wound healing rates are determined by monitoring ring closure once the ring magnet is removed. Two individual fibroblast cell models, HT-1080 fibrosarcoma cells and primary dermal fibroblasts, were tested to compare wound healing rates between cancer cell line and primary cell models. Cocultures containing fibroblasts and keratinocytes were also examined to ascertain whether more *in vivo*-like cell models affect wound healing rates. Automated kinetic imaging was performed using a novel cell imaging multimode reader to track ring closure at regular intervals during the incubation period. The combination provides an easy-to-use, robust method to generate accurate and repeatable results of the effect that new test molecules have on important wound healing applications.

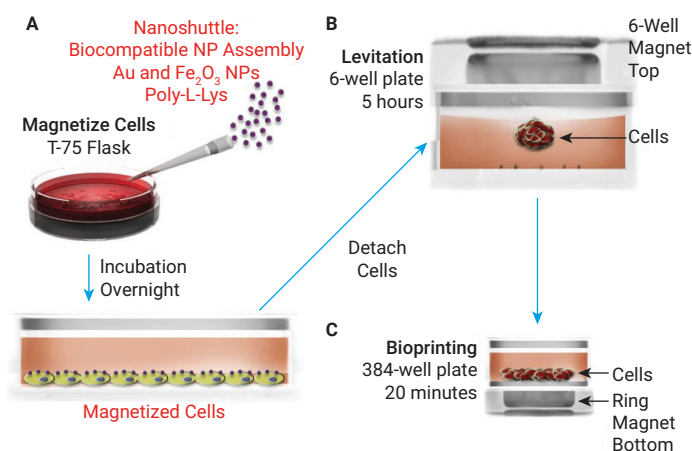


Figure 1. BiO Assay Kit protocol. The 384-Well BiO Assay Kit uses the NanoShuttle-PL nanoparticle assembly to (A) magnetize cells. After incubation, (B) cells are detached, resuspended in a cell-repellent plate, and magnetically levitated to aggregate and induce ECM. After breaking up the aggregates, (C) single cells are transferred to a 384-well cell-repellent plate placed atop a 384-well ring magnet, where they aggregate at the well bottom in the shape of the magnet. Following aggregation, the plate is removed from the magnet before placement into the imager. Cell rings will contract over time corresponding to wound healing rate of the cell model and well treatment.

Materials and methods

Materials

Assay and experimental components

The 384-Well BiO assay kit (GBO part number 781846, consisting of two vials NanoShuttle-PL, 6-well levitating magnet drive, 384-well spheroid and holding magnet drives (2), 96-well deep well mixing plate, 6-well and 384-well clear cell repellent surface microplates), prototype 384 well ring drive, and extra cell repellent surface 6-well (GBO part number 657860) and 384-well black μ Clear. Microplates (GBO part number 781976) were generously donated by Nano3D Biosciences, Inc. (Houston, TX) and Greiner Bio-One, Inc. (Monroe, NC).

The known inhibitor Cytochalasin D (part number 1233) was purchased from R&D Systems (Minneapolis, MN).

Cells

HT-1080 fibrosarcoma cells (part number CCL-121) and immortalized keratinocytes (part number CRL-2309) were obtained from ATCC (Manassas, VA). RFP expressing human neonatal dermal fibroblasts (part number cAP-0008RFP) were obtained from Angio-Proteomie (Boston, MA).

Agilent BioTek Cytation 5 cell imaging multimode reader

Cytation 5 is a modular multimode microplate reader combined with automated digital microscopy. Filter- and monochromator-based microplate reading are available, and the microscopy module provides up to 60x magnification in fluorescence, brightfield, color brightfield, and phase contrast. With special emphasis on live cell assays, Cytation 5 features temperature control to 65 °C, CO₂/O₂ gas control and dual injectors for kinetic assays, and is controlled by integrated Agilent BioTek Gen5 microplate reader and imager software. The instrument performed kinetic imaging of the 3D cell structure using brightfield and red fluorescent protein (RFP) imaging channels, and a 2x objective.

Methods

Assay procedure

T-75 flasks of cell cultures or cocultures were cultured to 80% confluence, then treated with 600 μL NanoShuttle-PL overnight at 37 °C/5% CO_2 . After incubation, cells were trypsinized, washed, and incubated for 3 to 5 minutes at 37 °C/5% CO_2 . Cells were removed from the flasks and added to the 6-well cell repellent plate at a concentration of 1.2×10^6 cells/well. A 6-well magnet drive was placed atop the well plate to levitate the cells, where they aggregated into 3D structures and induced ECM formation during a five-hour incubation at 37 °C/5% CO_2 . After incubation, the cells and ECM were broken up, resuspended and added to 384-well cell repellent plate wells at a total concentration of 1.0×10^5 cells/well, in a volume of 37.5 μL , along with 12.5 μL of 4x cytochalasin D, for a final 1x concentration of 10-0 μM . For tests involving cocultured fibroblasts and keratinocytes, 5.0×10^4 cells from each cell type were added to the well to create the 1.0×10^5 total cell number. A 384-well ring magnet drive was placed below the well plate, and the assembly was incubated at 37 °C/5% CO_2 for 20 minutes to allow cells within each well to aggregate into the magnet's ring shape. Following the completion of the aggregation process, the plate was removed from the ring magnet drive and placed into the Cytation 5. Automated brightfield imaging, using a 2x objective, captured ring closure on all wells every 30 minutes for 16 hours. Automated fluorescence imaging, using the RFP channel, was also performed on wells containing primary fibroblasts as they constitutively express RFP.

Results and discussion

Label-free image-based 3D wound healing monitoring

Following the assay protocol, 100,000 total HT-1080 cells/well, were added to the 384-well cell repellent plate where kinetic brightfield imaging was performed. As illustrated by the lack of ring structure change over time (Figures 2A and 2B), cytochalasin D inhibits HT-1080 wound healing. Conversely, Figures 3A to 3E illustrate that the HT-1080 cellular ring contracts in an uninhibited setting, as seen during *in vitro* wound healing, and also demonstrates the ability of Cytation 5 to track uninhibited cellular ring movement throughout the entire incubation.

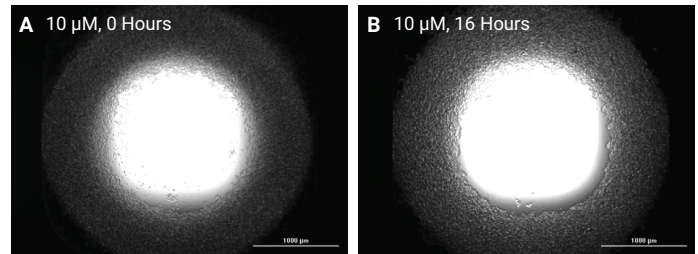


Figure 2. HT-1080 cells treated with cytochalasin D. 2x brightfield images captured from individual wells of HT-1080 cells treated and incubated as follows: (A) 10 μM cytochalasin D, 0 hours incubation; (B) 10 μM cytochalasin D, 16 hours incubation.

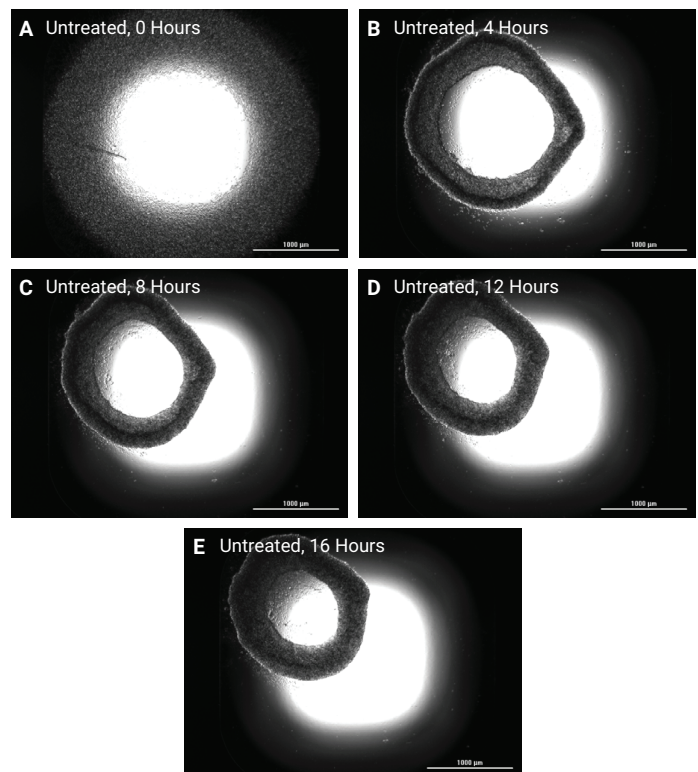


Figure 3. Untreated (0 μM cytochalasin D) HT-1080 cells. 2x brightfield images captured from individual wells of untreated HT-1080 cells incubated for (A) 0 hours; (B) 4 hours; (C) 8 hours; (D) 12 hours; (E) 16 hours.

Next, wound healing extent was analyzed using Cytation 5 brightfield imaging. Using the parameters in Table 1, object masks were automatically placed around 3D cellular structures (Figure 4) to track parameters such as object size, area, and total brightfield signal over the total incubation time. As seen in the images from Figures 3 and 4, the ring structures begin as large objects and then close over time in response to the combined forces pulling on each individual cell. For the cell analysis algorithms of the Agilent Biotek Gen5 software to properly identify each ring as a single object, certain adjustments are necessary. Minimum and maximum object size are increased to encompass the smallest and largest ring structures. *Split touching objects* is unchecked and *Include edge objects* is checked to further enhance object identification. Finally, due to large object size, the advanced *Background flattening size* parameter is also dramatically increased. This ensures that the image information remains for proper identification of rings that can be over 2,000 μm in size. In addition, because of the use of brightfield imaging and slight variations in intensity throughout the ring structure, *Image smoothing strength* is set to a high value. This and the background flattening size setting also aid in the identification of accurate single objects per well. Taken together each analysis parameter allows the identified signal threshold value to consistently place object masks around the ring, particularly when only subtle differences exist between background and ring intensity levels. It is important to note that cellular analysis parameters may vary depending on cell type. Optimization of parameters should always be performed when working with untested cell models. Object area was used for all analyses.

Table 1. Agilent BioTek Gen5 brightfield cellular analysis parameters. As cell types vary, parameter optimization should always be performed with untested cell models.

Brightfield Primary Cellular Analysis Parameters	
Threshold	16,000
Minimum Object Size	500 μm
Maximum Object Size	3,000 μm
Bright Objects on a Dark Background	Unchecked
Split Touching Objects	Unchecked
Include Edge Objects	Checked
Advanced Options	
Evaluate Background On	20% of lowest pixels
Image Smoothing Strength	10
Background Flattening Size	10,000 μm

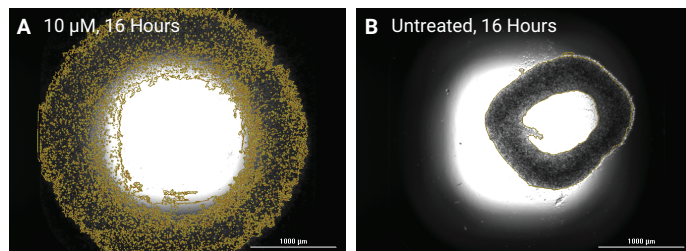


Figure 4. HT-1080 cellular analysis using the Agilent BioTek Cytation 5 cell imaging multimode reader 2x brightfield imaging. Object masks shown on cells treated and incubated as: (A) 10 μM cytochalasin D, 16-hour incubation; (B) 0 μM cytochalasin D (untreated), 16-hour incubation.

Finally, Cytation 5 calculated the HT-1080 3D cell ring structure's total area for each 30-minute time point, for real-time wound healing analysis. The percent of initial area decreases with time as lower cytochalasin D concentrations are added to the well. Data normalization was carried out by comparing total area at each time point to initial area (Figure 5). Also, per Figure 6, Cytation 5 can be used to calculate cytochalasin D IC_{50} values using single time point data.

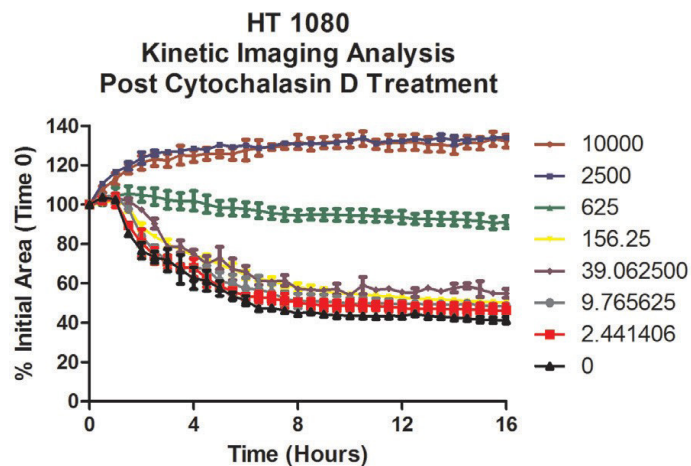


Figure 5. HT-1080 wound healing analysis using dose-dependent percent of initial area. Values represent nM cytochalasin D concentrations tested per well.

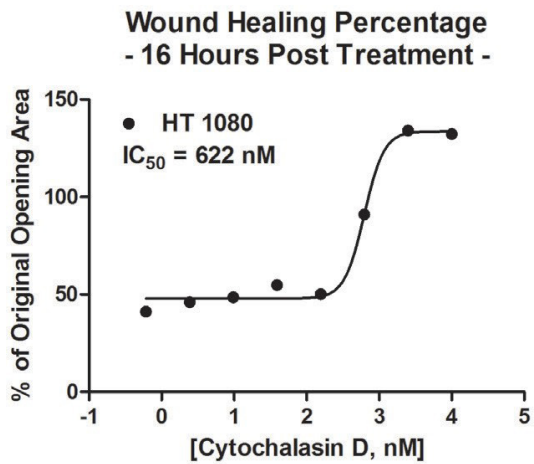


Figure 6. HT-1080 post incubation wound healing IC_{50} calculation.

Primary fibroblast comparison

Using immortalized cancer cell lines as surrogate models for primary cells affords the advantage of providing a continuous cell source for experimental purposes. However, internal changes in the cancer cell may modify the migratory characteristics of the cell model as seen by Varani, *et al.* when comparing normal mouse embryo fibroblasts and mouse fibrosarcoma cells.¹ Human dermal fibroblasts were tested using conditions previously described to examine potential differences between primary cells and the HT-1080 fibrosarcoma cell line.

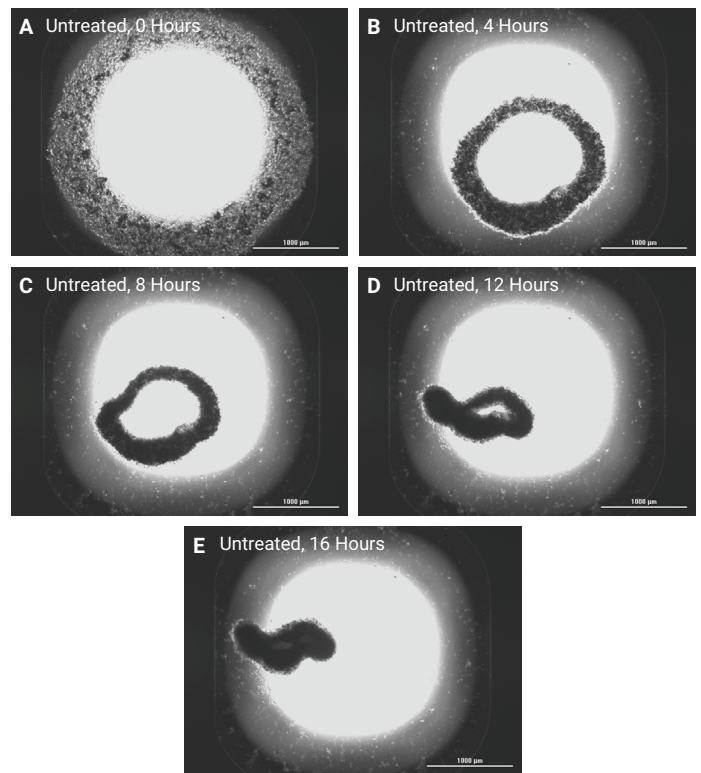


Figure 7. Untreated ($0 \mu\text{M}$ cytochalasin D) primary fibroblasts cells. 2x brightfield images captured from individual wells of untreated primary fibroblast cells incubated for (A) 0 hours; (B) 4 hours; (C) 8 hours; (D) 12 hours; (E) 16 hours.

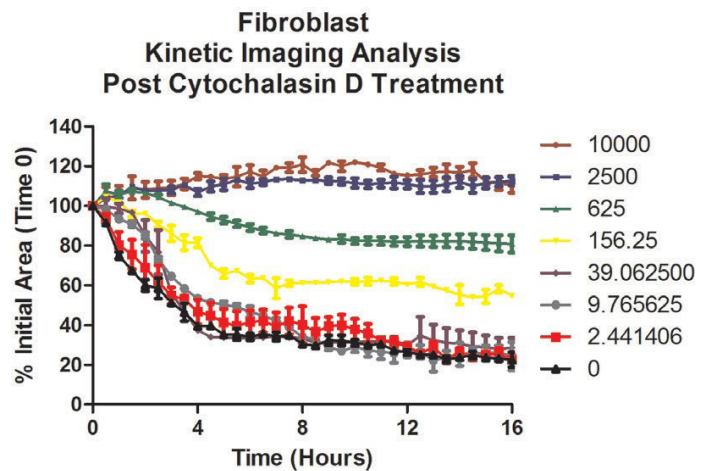


Figure 8. Kinetic primary fibroblast wound healing analysis using dose-dependent percent of initial area.

The Cytation 5 was again used to calculate the 3D cell ring total area, created using primary fibroblasts, for wells at each 30-minute time point. A greater percentage of wound healing was seen using primary cells compared to the cancer cell line. Cytochalasin D IC_{50} values, using the primary fibroblasts, were calculated (Figure 9) and demonstrated a left shift when compared to values generated with the cancer cell line.

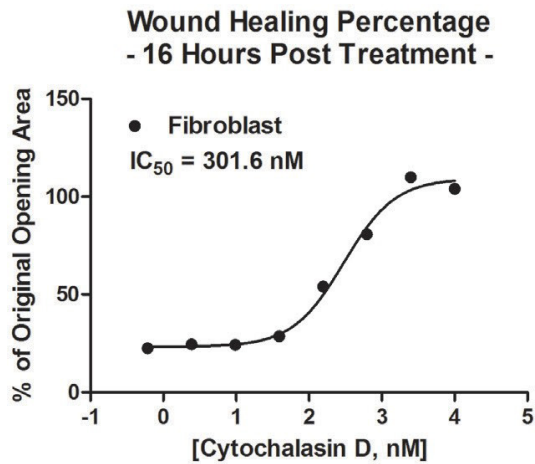


Figure 9. Primary fibroblast wound healing IC_{50} calculation.

Wound healing analysis can also be performed using Cytation 5 fluorescence imaging channels for cells labeled with a fluorescent probe or that constitutively express a fluorescent protein, such as the RFP expressing primary fibroblasts used here. Automated object masks from Table 2 were used to track changes in the 3D cell ring area (Figure 10). The enhanced contrast provided by fluorescence relative to brightfield microscopy allowed the use of lower threshold and less aggressive background adjustment and smoothing analysis parameters. Also, equivalencies were seen when comparing kinetic wound healing patterns (Figure 11) and cytochalasin D IC_{50} values (Figure 12) from brightfield and RFP signals.

Table 2. Agilent BioTek Gen5 RFP cellular analysis parameters. As cell types vary, parameter optimization should always be performed with untested cell models.

RFP Primary Cellular Analysis Parameters	
Threshold	5,000 RFU
Minimum Object Size	500 μm
Maximum Object Size	3,000 μm
Bright Objects on a Dark Background	Checked
Split Touching Objects	Unchecked
Include Edge Objects	Checked
Advanced Options	
Evaluate Background On	5% of lowest pixels
Image Smoothing Strength	3
Background Flattening Size	Auto

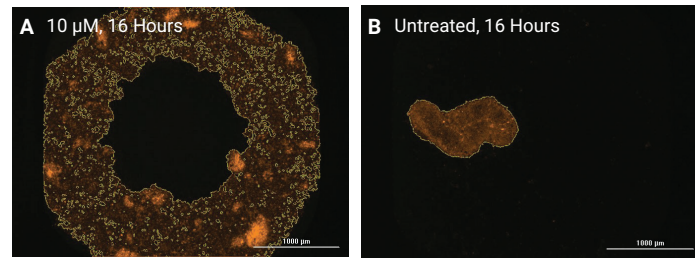


Figure 10. Primary fibroblast cellular analysis using the Agilent BioTek Cytation 5 cell imaging multimode reader 2x RFP imaging. Object masks shown on cells treated and incubated as: (A) 10 μM cytochalasin, 16-hour incubation; (B) 0 μM cytochalasin (untreated), 16-hour incubation.

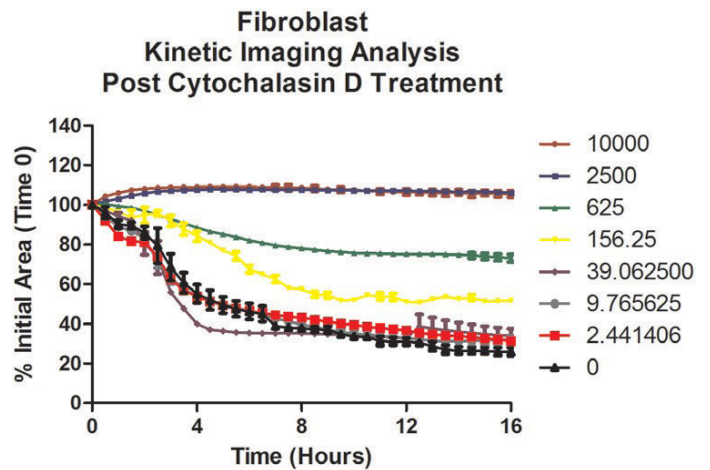


Figure 11. Kinetic primary fibroblast wound healing using RFP channel cellular analysis per cytochalasin D concentration treatment.

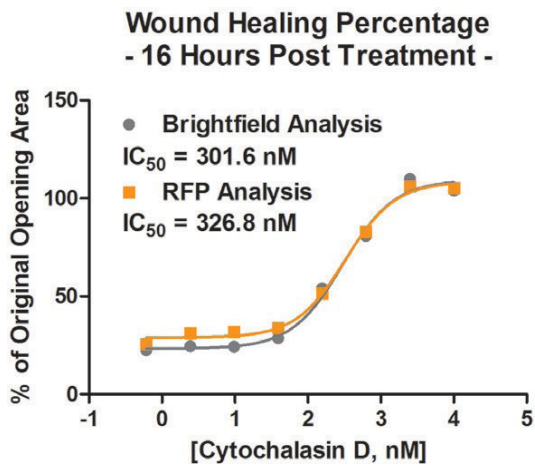


Figure 12. Comparison of primary fibroblast brightfield and RFP IC_{50} calculations.

Fibroblast and keratinocyte coculture analysis

Finally, cocultured wound healing was examined. Werner, *et al.* demonstrated that interactions between keratinocytes and fibroblasts dominate many phases of the wound healing process.² Therefore, incorporation of a coculture of these two cell types, as shown in Figure 13, may provide a more accurate representation of *in vivo* wound healing.

Figures 13 and 16, and the graph of uninhibited wound healing for all cell models in Figure 17, demonstrate that the fibroblast/keratinocyte coculture increased wound healing rates compared to fibroblasts alone or cancer cells. The cocultured 3D ring completely closes by the seventh hour, compared to moderate closure with the remaining cell models. Also, the HT-1080 IC_{50} curve was distinctly different from the other cell models, as seen in Figure 18. The cancer cell line demonstrates an extremely steep inhibitory curve and significantly less wound healing than the other two-cell models. These results validate the need for inclusion of appropriate cell models when performing wound healing analyses.

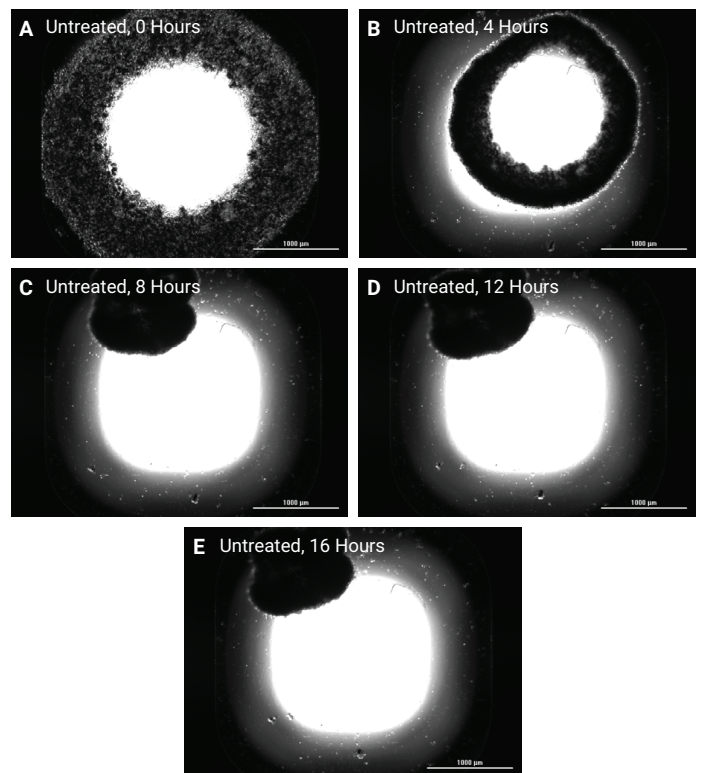


Figure 13. Untreated (0 μ M cytochalasin) primary fibroblasts and keratinocytes. 2x brightfield images captured from individual wells of untreated coculture incubated for (A) 0 hours; (B) 4 hours; (C) 8 hours; (D) 12 hours; (E) 16 hours.

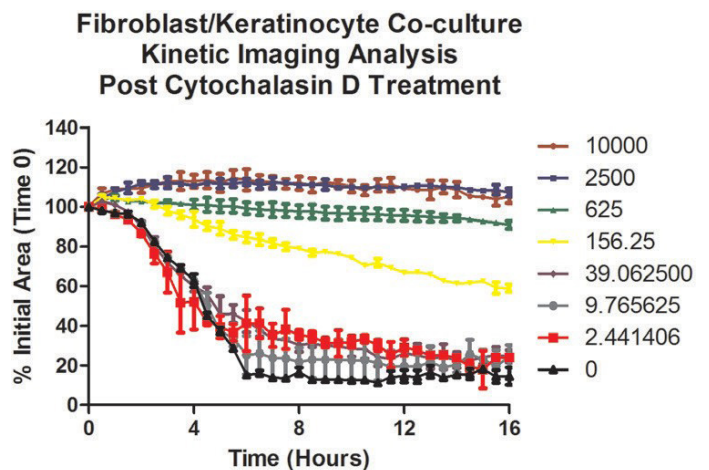


Figure 14. Kinetic coculture wound healing analysis using cytochalasin D dose-dependent percent of initial area.

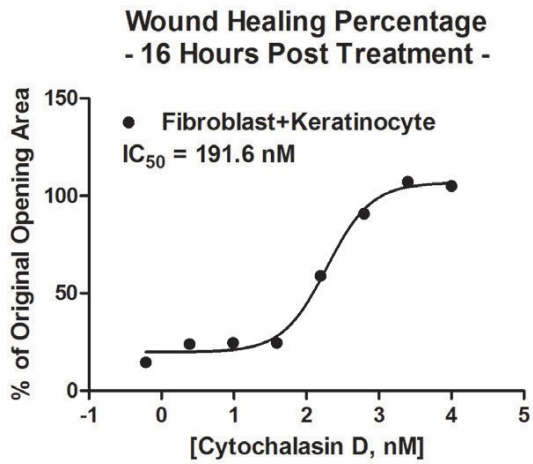


Figure 15. Coculture post incubation wound healing IC_{50} calculation.

Kinetic Analysis Uninhibited Wound Healing

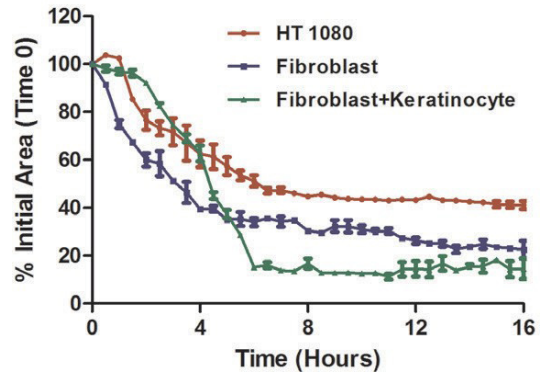


Figure 17. Wound healing rate cell model comparison.

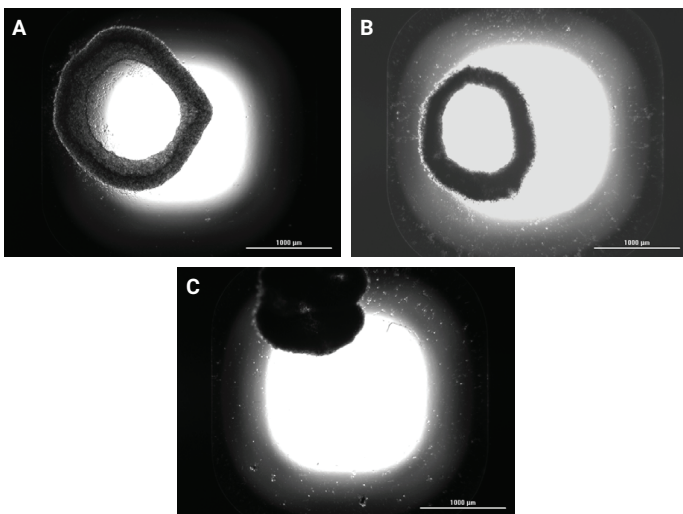


Figure 16. Comparison of cell model wound healing. 2x images captured from untreated (A) HT-1080 cells; (B) primary fibroblasts; (C) cocultured fibroblasts and keratinocytes; each incubated for 7 hours.

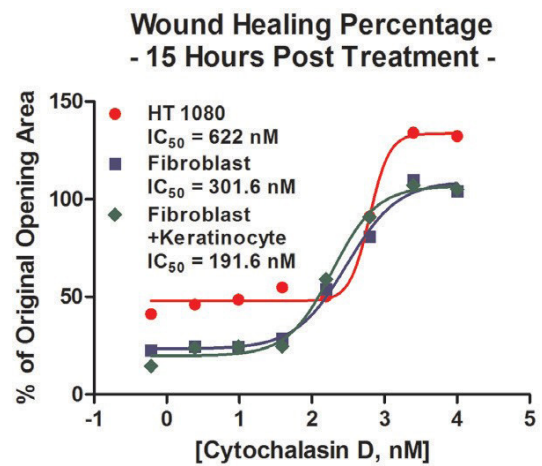


Figure 18. Wound healing IC_{50} cell model comparison.

Conclusion

The 384-Well BiO Assay Kit and NanoShuttle-PL particles manufactured by Nano3D Biosciences provide a simple, robust method to carry out 3D wound healing assessments, while incorporation of Greiner Bio-One cell-repellent surface 6-well and 384-well microplates allow efficient cell levitation for ECM creation, and high-throughput performance of the 3D wound healing assay. The addition of the Agilent BioTek Cytation 5 cell imaging multimode reader, with automated imaging and analysis in brightfield and fluorescence imaging channels, simplifies the assay process and increases analysis accuracy by removing manual determinations.

At the same time, use of primary cells may lead to a better understanding of *in vivo* dermal wound healing compared to cancer cells, and use of appropriate cell models, including primary and cocultured cells, may affect the extent and rate of wound healing, in addition to sensitivity to test molecules. The combination of assay method and automated imaging and analysis creates an easy to use, robust method to generate accurate and repeatable results when used for important dermal wound healing applications.

References

1. Varani, J.; Orr, W.; Ward, P. A. A Comparison of the Migration Patterns of Normal and Malignant Cells in Two Assay Systems. *Am. J. Pathol.* **1978**, *90*(1), 159–171.
2. Werner, S.; Krieg, T.; Smola, H. Keratinocyte-Fibroblast Interactions in Wound Healing. *J. Invest. Dermatol.* **2007**, *127*(5), 998–1008.

www.agilent.com/lifesciences/biotek

For Research Use Only. Not for use in diagnostic procedures.

RA44376.3079166667

This information is subject to change without notice.

© Agilent Technologies, Inc. 2016, 2022
Printed in the USA, June 23, 2022
5994-3364EN